Charge and thermoelectric transport mechanism in donor-acceptor copolymer films

Kaito Kanahashi,[1] Yong-Young Noh,[2] Won-Tae Park,[2] Hoichang Yang,[3] Hiromichi Ohta,[4] Hisaaki Tanaka,[5,*] and Taishi Takenobu[5,†]

[1]*Department of Advanced Science and Engineering, Waseda University, Tokyo 169-855, Japan*
[2]*Department of Chemical Engineering, Pohang University of Science and Technology, Pohang, Gyeongbuk 37673, Republic of Korea*
[3]*Department of Chemical Engineering, Inha University, 100 Inha-ro, Nam-gu, Incheon 22212, Republic of Korea*
[4]*Research Institute for Electronic Science, Hokkaido University, Sapporo 001-0020, Japan*
[5]*Department of Applied Physics, Nagoya University, Chikusa, Nagoya 464-8603, Japan*

(Received 4 July 2020; revised 13 October 2020; accepted 17 November 2020; published 7 December 2020)

Wearable thermoelectric conversion devices are one of the key technologies for future sustainable society, and flexible conducting polymer films are strong candidates for these applications. However, the thermoelectric transport mechanism of these materials is still unclear due to their unique disordered nature, in particular the poor interconnectivity between crystalline domains. Here, to overcome this limit, donor-acceptor (D-A) copolymer films are selected because of the efficient connection between domains via rigid tie molecules. We investigated their thermoelectric and carrier transport properties using the electrolyte-gating technique and perfectly described both of them based on the two-dimensional variable range hopping model with a linear density of states around the Fermi level energy. The present results provide a fundamental understanding of the thermoelectric physics in D-A copolymer films towards application in wearable devices.

DOI: 10.1103/PhysRevResearch.2.043330

I. INTRODUCTION

Recently, due to the rapid growth of the "Internet of Things" (IoT) concept, the 24-hour monitoring of health based on wearable devices has attracted much interest [1–3]. However, most IoT devices are still powered by batteries that require frequent recharging or replacement, and therefore, it is still difficult to continuously monitor physical and psychological conditions for a long time. To solve this power issue, one of the best technologies is wearable thermoelectric batteries, in which electric power is generated from a temperature difference between the body and ambient air.

Among various candidates, conducting polymers are one of the best materials for these applications because of their flexible film structure consisting of ordered rigid domains (fibrils or aggregates) and amorphous-like soft boundary region, as well as their light weight, printability, lower toxicity, and abundance of their composition atoms (mainly carbons and hydrogens). Although polymer films are promising for wearable devices, their thermoelectric performance is still too low to satisfy the required output power for microscale sensors and processors (1–10 μW) [3–6]. Consequently, guiding principles for achieving higher performance based on the physics of their thermoelectricity are significantly required.

In general materials, the relationship between the Seebeck coefficient, S, and the electrical conductivity, σ, is simply explained by their carrier transport mechanisms [e.g., metallic, thermally activated, and variable range hopping (VRH) transport], and this understanding has led to performance improvement [7,8]. In stark contrast, the thermoelectricity of conducting polymer films is not explained by their carrier transport mechanisms, and therefore, there are no clear guiding principles to design high-performance thermoelectric materials and devices.

In most conducting polymer films, their transport properties are described by thermally activated or VRH transport mechanisms arising from the temperature dependence of the conductivity [9–11], and these models suggest S-σ relationships of $S \propto \log \sigma$ or $S \propto |\ln(\sigma/\sigma_0)|^x$. Here, σ_0 is a temperature-independent factor, and x is dependent on the shape of the density of states and the dimensionality of carrier transport. However, the experimentally observed S-σ relationship of conducting polymers has an unusual power-law dependence of $S \propto \sigma^{-1/s}$, where s takes a value of 3 or 4 in most cases [12,13], meaning a significant lack of a fundamental understanding of the physics of their thermoelectricity.

Very recently, we proved that the unusual power-law S-σ relationship of semicrystalline poly[2,5-bis(3-alkylthiophen-2-yl)thieno(3,2-b)thiophene] (PBTTT) is determined *not* only by the crystalline domains *but* also by the boundary region [14]. Moreover, we proposed that the torsion of PBTTT molecules in the boundary region causes a negative effect on the transport properties, i.e., the torsion of the backbone at the domain boundaries prevents the efficient interdomain

*Corresponding authors: htanaka@nuap.nagoya-u.ac.jp
†takenobu@nagoya-u.jp

transport as demonstrated by several semicrystalline polymer devices [15–17]. Consequently, these results critically indicate that reduction of the boundary effect is the key issue for fully understanding the thermoelectricity in conjugated polymers.

Motivated by this assumption, donor-acceptor (D-A) copolymers are selected as target materials because it is believed that their crystalline domains are microscopically bridged via rigid and nearly torsion-free tie molecules (tie chains) [18–22]. Among the variety of D-A copolymers, thiophene-flanked diketopyrrolopyrrole (DPP)-based copolymers are one of the most frequently used materials owing to their high transport performance [23–27]. These polymers exhibit high backbone planarity due to the so-called "noncovalent conformational locking effect" [26] through the weak O–H hydrogen bonding between DPP and thiophene subunits [28,29]. Such planar polymers exhibit the higher mobility ($>0.1\,\mathrm{cm^2\,V^{-1}\,s^{-1}}$) than the highly-crystalline polymers with large backbone torsions such as poly(3-hexylthiophene) (P3HT) and PBTTT due to the improved interconnectivity between the crystalline domains or aggregates, as is also demonstrated for various D-A polymers [16–30], some of which exhibits high mobility even though the molecular organization is nearly amorphous [18,19]. Therefore, charge transport process in the thiophene-flanked DPP-based D-A polymers will not be affected by boundaries and these materials are regarded as one of the best materials for thermoelectric research. However, to our best knowledge, there is no previous report of the thermoelectric mechanism for this class of materials.

In the present study, we investigate both the thermoelectric properties and the charge transport mechanism of D-A copolymer films using the electrolyte-gating technique to control their carrier concentration. All experimental results, such as the temperature (T)-σ and S-σ relationships, are completely explained within the framework of the conventional VRH model, and this study obviously concludes that the interconnection between domains is a key element to understand the physics of the thermoelectricity in conducting polymer films.

II. EXPERIMENTAL METHODS

A. Sample preparation

D-A copolymers of poly(2,5-bis(2-octyldodecyl)-3-(5-(thieno[3,2-b]thiophene-2,5-yl)thiophene-2-yl)-6-(thiophen-2,5-yl)pyrrolo[3,4-c]pyrrole-1,4(2H,5H)-dione) (DPPT-TT), poly(3-(2,2′-bithiophen-5,5′-yl)-2,5-bis(2-octyldodecyl)-6-(thiophen-2,5-yl)pyrrolo[3,4-c]pyrrole-1,4(2H,5H)-dione) (PDPP3T), and poly(3−(2,2′:5′,2″-terthiophen-5,5″-yl)-2,5-bis(2-octyldodecyl)-6-(thiophen-2,5-yl)pyrrolo[3,4-c]pyrrole-1,4(2H, 5H)-dione) (PDPP4T) were purchased from Ossila Ltd. The gap energies between the highest occupied molecular orbital (HOMO) and the lowest unoccupied molecular orbital (LUMO) of the target polymers are 1.26 eV (DPPT-TT), 1.56 eV (PDPP3T), and 1.2 eV (PDPP4T) [20]. First, Au/Ni (15/5 nm) electrodes were thermally evaporated on a glass substrate (Corning XG) with a typical size of 1 cm × 1 cm × 0.5 mm. The channel length and channel width were 0.4 and 2 mm, respectively. Second, the glass substrate with electrodes was cleaned in deionized water, acetone, and 2-propernol for 10 minutes each and by ozone-plasma treatment for 20 minutes. Third, we prepared 5 mg $\mathrm{ml^{-1}}$ *o*-dichlorobenzene solutions of D-A copolymers. Then, a conducting polymer layer was fabricated by the spin-coating method (1500 rpm for 150 s). The resultant D-A copolymer films were annealed at 100 °C for 30 minutes in a N_2-filled glove box. Finally, we formed an ion gel film composed of the ionic liquid (N,N-diethyl-N-(2-methoxyethyl)-N-methylammonium bis-(trifluoromethylsulfonyl)-imide) [DEME][TFSI] and an organic polymer poly(vinylidene fluoride-co-hexafluoropropylene) (P(VDF-HFP)) (weight ratio of [DEME][TFSI]/P(VDF-HFP) = 1) on another glass substrate by spin-coating (6000 rpm for 120 s). The ion gel film was annealed at 70 °C for 30 minutes and then transferred onto the conducting polymer films.

B. Measurement of the Seebeck coefficient and the four-point-probe electrical conductivity

Thermoelectric measurements were performed in a N_2-filled glove box at room temperature. The electrolyte-gating transistor sample was fixed on two Peltier elements (Laird Technologies, CP1.0-31-05L) to generate a temperature difference (ΔT). Moreover, two K-type (alumel–chromel, diameter of 100 μm each) thermocouples (Sakaguchi EH VOC Corp. TCKT0051) were placed on the surface of the polymer films to measure the temperatures of the source (T_A) and drain (T_B) electrodes. The measured temperature was monitored by a temperature controller (Lakeshore, model 335). We set several values of $\Delta T (= T_A - T_B)$ using the two Peltier elements and simultaneously monitored the thermoelectromotive force (ΔV) through the source and drain electrodes using a nanovoltmeter (Keysight 34420A). Then, the Seebeck coefficient was determined by the slope of the relationship between ΔV and ΔT based on the definition of $S = \Delta V/\Delta T$. It should be noted that the linearity of the ΔV–ΔT profiles was significantly degraded when the channel resistance between the source and drain electrodes was higher. Thus, the Seebeck coefficient at lower electrical conductivities ($<0.1\,\mathrm{S\,cm^{-1}}$) was not measured in this study. After collecting the Seebeck coefficient results, the four-point-probe electrical conductivity was estimated from current-voltage curves by applying a drain voltage from –0.1 to 0.1 V. The voltage drop between the two voltage probes in the four-point-probe configuration was monitored using a nanovoltmeter (Keysight 34420A).

C. Low-temperature measurements:

Low-temperature experiments were performed in a physical property measurement system (PPMS, Quantum Design, model 6000). A gate voltage was applied at 300 K with application of a −10 mV drain voltage. The transistor characteristics were monitored by a semiconductor parameter analyzer (Agilent Technologies, Inc. B1500A). Simultaneously, the voltage drop between the two voltage probes in the four-point-probe configuration was measured using a nanovoltmeter (Hewlett-Packard 34420A). We performed the low-temperature measurements for $V_\mathrm{G} = -1.5$ V, at which the

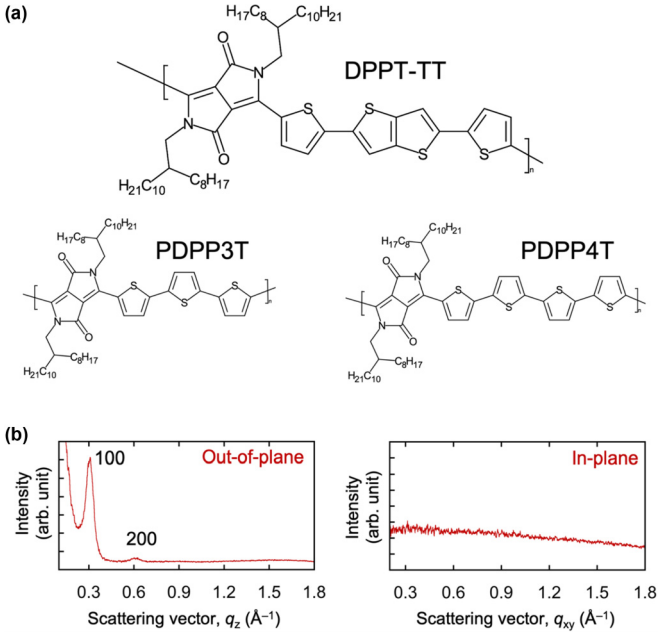

FIG. 1. Chemical structures of D-A copolymers and film characterization. (a) Molecular structures of DPPT-TT, PDPP3T, and PDPP4T. (b) XRD out-of-plane and in-plane profiles obtained from the optimized DPPT-TT film as a function of the scattering vector.

gate current is lower than the drain current. The temperature control conditions were 2 K min^{-1} above 100 K and 1 K min^{-1} below 100 K.

III. EXPERIMENTAL RESULTS

Among the various D-A copolymers, we mainly focused on DPPT-TT [Fig. 1(a)], which is one of the most typical materials within the DPP family. First, we fabricated field-effect transistors (FETs) of DPPT-TT films and optimized the annealing temperature based on their carrier mobilities (see Appendix A). In parallel with the optimization, we verified the film quality by atomic force microscopy and x-ray diffraction (XRD) measurements. Figure 1(b) shows out-of-plane and in-plane XRD patterns obtained for the optimized DPPT-TT film. As shown in Fig. 1(b), diffraction peaks of $h00$ are observed perpendicular to the substrate surface, and the corresponding interplanar spacing is 20.4 Å, which agrees with the interlamellar distance of DPPT-TT and proves the formation of a crystalline lamellar structure similar to those observed in the previous report [23–25]. It is known that in the case of DPP-based monomer or oligomer films there can appear some polymorphs with different transport properties [31], whereas no signature of such polymorph is observed in the present polymer film. This result indicates that the present DPPT-TT has an edge-on orientation, indicating in-plane two-dimensional (2D) hopping transport within the crystalline domains. On the other hand, there is no obvious (010) peak along the specific in-plane direction, suggesting a small in-plane domain size and low coherence of the $\pi-\pi$ stacking structure. Despite such low in-plane crystallinity of the DPPT-TT film, the FET mobility exceeds 0.2 cm^2 V^{-1} s^{-1} (see Appendix A), which is comparable to or even higher than those of semicrystalline PBTTT and P3HT films [32–34]. The observed high mobility even though the low crystallinity can reasonably been explained in terms of the high planarity of the backbone conformation with the torsion angle of at most 4° between the structural subunits [28]; the highly planar backbones can electrically interconnect the adjacent crystalline domains efficiently to suppress the effect of domain boundaries on the macroscopic charge transport [16–18], suggesting that the negative effect of the boundaries on the transport process observed in the case of PBTTT due to the inferior interdomain connection by the large backbone torsion is suppressed.

TABLE I. Fitting results of the Zabrodskii analysis. The values of the Seebeck coefficient of sample no. 3 at each room-temperature electrical conductivity are estimated from the experimentally observed S-σ relationships in sample no. 1 and sample no. 2. The results of PBTTT and P3HT are also shown [9,10].

V_G (V)	σ_{300K} (S cm^{-1})	σ_0 (S cm^{-1})	T_0 (K)	Estimated S (μV K^{-1})
–1.6	5	4038	11481	100
–1.7	39	1591	3498	53
–1.8	92	1204	1648	34
–1.9	127	1160	1273	27
PBTTT [9]	120	2000	19 400	–
P3HT [10]	100	840	6300	–

Figure 2(a) shows a schematic illustration of the electrolyte-gated transistor using the DPPT-TT film. The gate dielectric layer is an ion gel film composed of an ionic liquid, [DEME][TFSI], and an organic polymer, P(VDF-HFP). Figure 2(b) displays the thermoelectric measurement setup in a N_2-filled glove box at room temperature [35]. As shown in Fig. 2(b), two thermocouples were directly placed onto the surface of polymer films to monitor the temperature of the source (T_A) and drain (T_B) electrodes. Figure 2(c) presents the transfer curve of the DPPT-TT electrolyte-gated transistor (sample no. 1), in which clear transistor operation is observed. Moreover, there is a large hysteresis between forward and backward sweeps, possibly due to the doping and dedoping processes of anion molecules. However, it should be noted that the penetration of anion molecules into the polymer film does not degrade the crystalline domains, which has been verified by XRD measurements performed under electrochemical doping conditions (see Appendix B).

Along with the transistor measurements, we performed both Seebeck coefficient and four-point-probe electrical conductivity measurements at fixed gate voltages. Figures 2(d) and 2(e) summarize the electrical conductivity dependences of the Seebeck coefficient and the power factor in DPPT-TT films (samples no. 1 and no. 2), respectively. For comparison, we also fabricated electrolyte-gated transistors using other D-A copolymers, such as PDPP3T and PDPP4T [Fig. 1(a)]. As shown in Fig. 2(d), for all of these D-A copolymers, the collected highest conductivities at 300 K (σ_{300K}) are greater than 100 S cm^{-1} and are comparable to those of semicrystalline PBTTT and P3HT films (Table I) [9,10] even though the crystallinity of the present polymers is lower than these

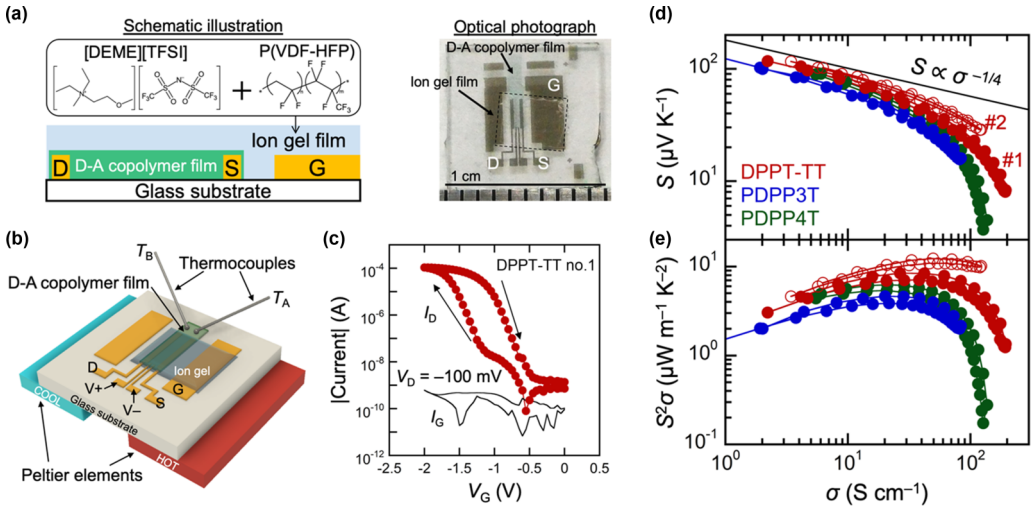

FIG. 2. Thermoelectric measurement of donor-acceptor copolymer films using the electrolyte-gating technique. (a) Schematic cross-sectional illustration of the electrolyte-gating transistor. An optical photograph of the DPPT-TT sample is also provided, with the dotted frame being the region of the ion gel. The scale bar corresponds to 1 cm. (b) Schematic illustration of the thermoelectric measurement setup combined with electrolyte-gating transistors in a N_2-filled glove box at room temperature. (c) Transistor characteristics of the DPPT-TT electrolyte-gating transistor (sample no. 1) with application of a constant drain voltage (V_D) of −100 mV. (d) S-σ relationships in D-A copolymer films (DPPT-TT, PDPP3T, and PDPP4T). The relationship of $S \propto \sigma^{-1/4}$ is also indicated. (e) Power factors in D-A copolymers as a function of σ.

semicrystalline polymers, again proving the less negative effect from boundaries due to the efficient connection between domains via tie molecules. These D-A copolymer films exhibit similar and reversible thermoelectric features with less hysteresis, indicating that the observed S-σ relationships are intrinsic properties of D-A copolymers. Moreover, as shown in Fig. 2(e), the power factors of these films are well maximized by the electrolyte-based carrier doping, which has also been demonstrated in PBTTT very recently [14].

To determine the charge transport mechanism of DPPT-TT films, we also measured the temperature dependences of the four-point-probe electrical conductivity in the DPPT-TT electrolyte-gated transistor (sample no. 3) at various gate voltages. The temperature range was set below 270 K, at which the magnitude of the gate leakage current is less than 1 nA. As shown in Fig. 3(a), the DPPT-TT film exhibits insulating

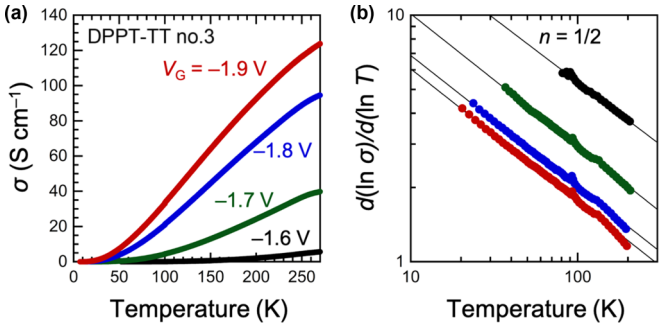

FIG. 3. Charge transport properties of DPPT-TT films investigated by using electrolyte-gating transistors. (a) Temperature dependences of the four-point-probe electrical conductivity (σ) at various gate voltages (V_G) in the DPPT-TT electrolyte-gating transistor (sample no. 3). (b) Zabrodskii plots at various gate voltages. Black solid lines correspond to the results of $n = 1/2$.

behavior up to the maximum electrical conductivity, and the observed temperature dependences of the conductivity are not explained by thermally activated hopping transport (see Appendix C), even though it is one of the typical transport mechanisms in conducting polymers. Next, we also considered the VRH transport mechanism. Within the framework of the VRH model, the temperature dependence of the electrical conductivity is described as

$$\sigma(T) = \sigma_0 \exp\left[-\left(\frac{T_0}{T}\right)^n\right], \tag{1}$$

where n correlates with the dimension of the transport system and T_0 is interpreted as an effective energy separation between localized states [36,37]. To determine the exponent n, we performed Zabrodskii analysis, as shown in Fig. 3(b) [38]. In the Zabrodskii plot, n is equal to the slope of the relationship between $\log d(\ln\sigma)/d(\ln T)$ and $\log T$. As shown in Fig. 3(b), linear trends corresponding to $n = 1/2$ are clearly observed up to 200 K at all gate voltages. Notably, in semicrystalline PBTTT and P3HT films, although the temperature dependences of their conductivity are also explained by the VRH model, the obtained n is dependent on both the doping level and temperature, making it difficult to analyze the S-σ relationship of these materials based on the VRH model [9,10]. In stark contrast, the doping level and temperature-independent behavior of the constant $n = 1/2$ in DPPT-TT films gives us the opportunity to understand both the thermoelectric properties and the charge transport mechanism within the framework of the VRH model.

To gain more insight into the transport mechanism in DPPT-TT films, we summarize the fitting results of the Zabrodskii analysis in Table I. First, the values of T_0 are strongly gate-voltage dependent. This behavior can be understood based on high-density electrochemical carrier doping,

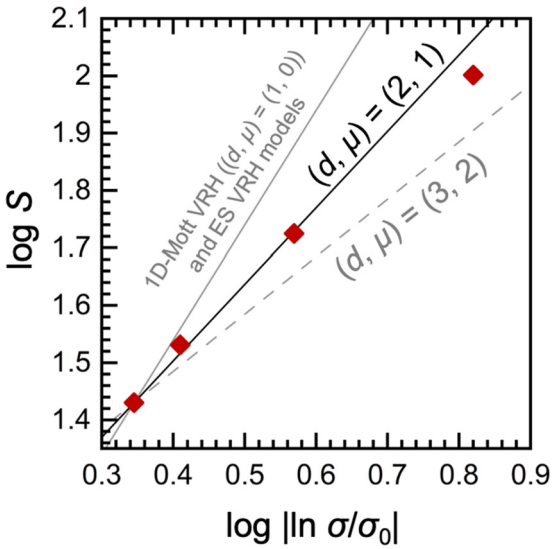

FIG. 4. Relationship between log S and log $|\ln(\sigma/\sigma_0)|$. The predicted slopes for the pairs of $(d, \mu) = (1, 0)$, (2, 1), and (3, 2) are also indicated.

which leads to an increase in the density of localized states at the Fermi level and a decrease in the energy separation between localized states. Second, the T_0 values at all gate voltages are greater than room temperature, which supports VRH transport with constant $n = 1/2$ up to room temperature. Third, as summarized in Table I, among the DPPT-TT, PBTTT, and P3HT films with similar room-temperature conductivity, the T_0 of the DPPT-TT film is smaller than those of the PBTTT and P3HT films, concluding that the localization effect at boundaries ($\sim T_0$) in the DPPT-TT film is suppressed by the more efficient connection between domains via tie molecules.

Since we described the T-σ relationship very well, we tried to understand the S-σ relationship of DPPT-TT films [Fig. 2(d)] based on the VRH model. Generally, the condition of $n = 1/2$ is interpreted in terms of the one-dimensional (1D) Mott VRH model or Efros-Shklovskii (ES) VRH model, and both of these models predict an identical S-σ relationship (see Appendix D) of [37–39]:

$$S_{\text{1D Mott VRH}} = S_{\text{ES VRH}} = \frac{k_B^2 T}{8e}\left(-\ln\frac{\sigma}{\sigma_0}\right)^2 \frac{\partial \ln \sigma_E(E)}{\partial E}\bigg|_{E=E_F}, \tag{2}$$

where k_B, e, σ_E, and E_F are the Boltzmann constant, the elementary charge, the spectrum conductivity, and the Fermi level energy, respectively. Consequently, under the condition of a constant $[\partial \ln \sigma_E(E)/\partial E|_{E=EF}]$, this equation predicts an $S - |\ln(\sigma/\sigma_0)|^x$ relationship with a power of $x = 2$. Based on this idea, we prepared the logarithmic plot of S versus $|\ln(\sigma/\sigma_0)|$, calculated from the room-temperature S-σ relationship [Fig. 2(d), samples no. 1 and no. 2] and the temperature dependence of σ (Fig. 3, sample no. 3). These parameters are also summarized in Table I [40]. As shown in Fig. 4, although we obtained an x-power-law relationship between the experimental S and $|\ln(\sigma/\sigma_0)|$, our experimental results do not follow the slope of 2, suggesting that the thermoelectric mechanism in DPPT-TT films is not simply explained by the 1D Mott VRH model or ES VRH model.

Therefore, to understand the S-σ relationship of DPPT-TT films, we extended our analysis to the general VRH model, in which n is described by $(1 + \mu)/(1 + \mu + d)$, where μ represents the shape of the density of states around the Fermi level energy [i.e.,$D(E) \propto (E–E_F)^\mu$] [37,41]. Based on this primitive expression, the pairs of (d, μ) corresponding to $n = 1/2$ are limited to (1, 0), (2, 1), and (3, 2). Moreover, the theoretical S-σ relationship in the Mott VRH transport system is predicted to be

$$S_{\text{Mott VRH}} = \frac{k_B^2 T}{2e}\frac{1}{(1+d)^2}\left(-\ln\frac{\sigma}{\sigma_0}\right)^{\frac{2}{n(1+d)}} \frac{\partial \ln \sigma_E(E)}{\partial E}\bigg|_{E=E_F}. \tag{3}$$

Again, under the condition of a constant $(\partial \ln \sigma_E(E)/\partial E|_{E=EF})$, one can expect an x-power-law relationship between S and $|\ln\sigma/\sigma_0|$. In particular, with constant $n = 1/2$, the predicted slopes x of $S \propto |\ln(\sigma/\sigma_0)|^x$ for dimension $d = 1$, 2, and 3 correspond to 2, 4/3, and 1, respectively. On the other hand, as shown in Fig. 4, the experimentally obtained x obeys $1 < x < 4/3$, strongly indicating 2D or 3D VRH transport with nonzero μ. In addition, the gate-voltage-dependent decrease in T_0 (Table I) indicates an increase in the density of localized states at the Fermi level by carrier doping, and these results also agree with VRH transport with nonzero μ.

Among 2D and 3D VRH transport, the 2D nature of the hopping process is consistent with the edge-on orientation of the DPPT-TT molecules observed by XRD measurements (Fig. 1), where the conducting planes consisting of the $\pi-\pi$ stacking lie in the film plane and are separated by insulating alkyl chains along the film normal. Moreover, due to the definition of μ [i.e., $D(E) \propto (E–E_F)^\mu$], it is difficult to consider $\partial \ln \sigma_E(E)/\partial E|_{E=EF}$ as constant for $(d, \mu) = (2, 1)$ and $(d, \mu) = (3, 2)$. However, one can expect $\partial \ln \sigma_E(E)/\partial E|_{E=EF}$ to approach a constant value as the doping level (and σ) becomes sufficiently high. As shown in Fig. 4, the experimentally obtained x approaches 4/3 for smaller log $|\ln(\sigma/\sigma_0)|$, obviously indicating that both the thermoelectric properties and the charge transport mechanism of DPPT-TT films are completely explained within the framework of the VRH model with $(d, \mu) = (2, 1)$.

IV. DISCUSSION

Finally, we should discuss the guiding principles for higher performance in DPPT-TT films. Very simply, according to Eq. (3), one can predict a higher peak value of the power factor for a larger σ_0. Although σ_0 is generally proportional to the attempt-to-escape frequency, how to control σ_0 is still an open question. First, because interchain hopping is less effective than the intrachain hopping, large contribution of the interchain hopping in the spin-coated nonaligned film tends to result smaller σ_0. Thus, uniaxial alignment of the DPPT-TT chains will make σ_0 larger. Another approach might be to synthesize DPPT-TT molecules with a higher polymerization degree (longer polymer chain). Because in DPPT-TT films, efficient intradomain transport via 2D $\pi-\pi$ interactions and interdomain connection via rigid tie molecules are expected,

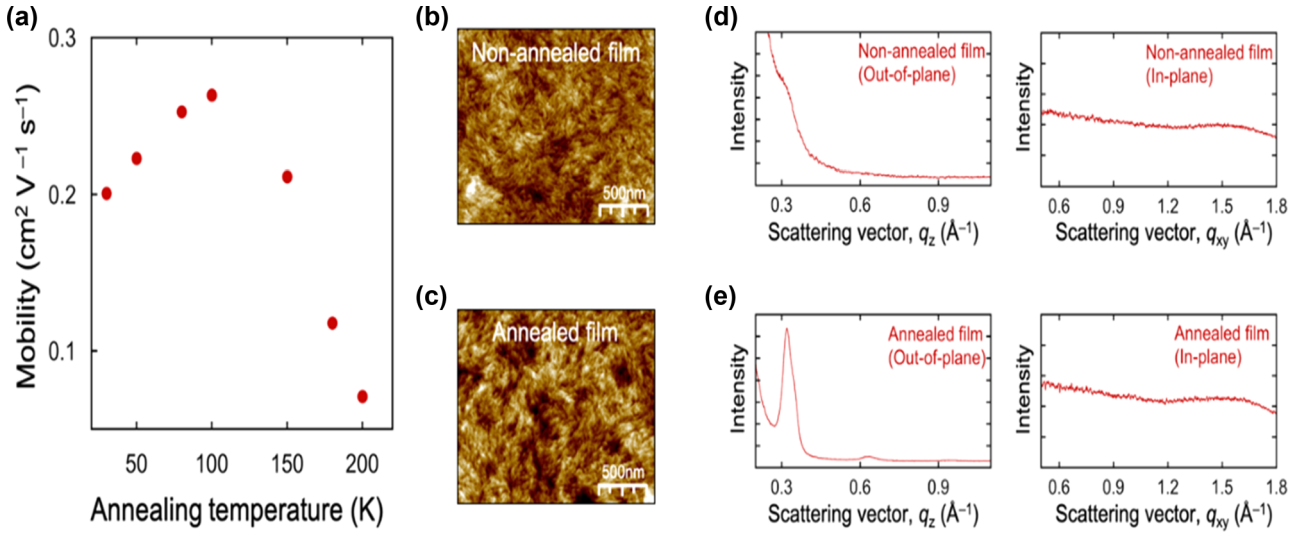

FIG. 5. Film optimization. (a) Field-effect mobilities of DPPT-TT film annealed at various temperatures. AFM topologies of the DPPT-TT films before (b) and after (c) annealing at 200 °C. (d) Out-of-plane and in-plane XRD profiles of the DPPT-TT film without annealing. (e) Out-of-plane and in-plane XRD profiles of the DPPT-TT film annealed at 200 °C.

one can guess the unique carrier transport, in which carriers might hop between DPPT-TT molecules when the chain ends of these molecules are located in the boundary region of adjacent domains [17]. Therefore, a longer polymer chain will decrease the number of hoping sites and thus increase σ_0. This assumption also agrees with the gate-voltage-dependent decrease of σ_0 (Table I) since penetrated cations and anions might degrade the carrier transport in the boundary region.

V. SUMMARY

In summary, both the thermoelectric and charge transport properties in D-A copolymer films were investigated by the electrolyte-gating method. In contrast to the unusual S-σ relationship empirically reported for most polymers, the S-σ relationship of D-A copolymer films is completely described by the conventional 2D variable range hopping process with a linear DOS at the Fermi energy, producing a peak structure of the power factor. The applicability of this simple framework is presumably ensured by the unique carrier transport within the D-A polymer thin film. This result opens a pathway to fully understanding the fundamental thermoelectric mechanism in conducting polymer films and provides a guideline to enhance their thermoelectric performances.

ACKNOWLEDGMENTS

We thank Dr. T. Hikage for the support with the x-ray diffraction experiments. H.T. and T.T. are partially supported by JSPS KAKENHI (Grants No. JP26102012, No. JP25000003, No. 19K22127, No. JP17H01069, No. 20H05867, and No. 20H05664) and JST CREST (Grant No. JPMJCR17I5). H.T. is partially supported by the Murata Science Foundation, Tatematsu Foundation and Iketani Science and Technology Foundation. H.O. is supported by JSPS KAKENHI (Grants No. JP17H01314 and No. 19H05791) and the Asahi Glass Foundation. H.Y. is thankful for the financial support from the Industrial Fundamental Technology Development Program (Grant No. 10051440) funded by the Ministry of Trade, Industry and Energy (MOTIE), Korea. This work was performed under the Research Program for Next Generation Young Scientists of "Network Joint Research Center for Materials and Devices: Dynamic Alliance for Open Innovation Bridging Human, Environment and Materials." This study was partially supported by Ministry of Science and ICT through the National Research Foundation, grant-funded by the Korea government (Grant No. 2017R1E1A1A01075360).

APPENDIX A: OPTIMIZATION OF THE ANNEALING TEMPERATURE AND FILM CHARACTERIZATION

We fabricated DPPT-TT field effect transistors on octyltrichlorosilane-treated Si/SiO_2 substrates. Figure 5(a) presents the field-effect mobility of DPPT-TT film in the linear region as a function of the annealing temperature. As shown in Fig. 5(a), the maximum mobility ($\sim$0.25 $cm^2\ V^{-1}\ s^{-1}$) is observed at an annealing temperature of 100 °C. Thus, we concluded that 100 °C was the optimum condition for the present study.

Next, we determined the influence of the annealing temperature on the film structure by atomic force microscopy (AFM, Multimode 8, Bruker) and x-ray diffraction (XRD) measurements. Figures 5(b) and 5(c) show the AFM topologies of nonannealed and 200 °C annealed DPPT-TT films, respectively. As shown in Fig. 5(b) and 5(c), there is no critical change between the two films. Moreover, Fig. 5(d) and 5(e) summarize the XRD profiles obtained from the two films. As shown in Figs. 5(d) and 5(e), although out-of-plane peaks are observed in both films, there are no clear in-plane peaks corresponding to π-π stacking. For the in-plane peaks, the shape in the high wave number region is different from that in Fig. 1(b), which is possibly due to the scattering from the glass substrate. According to these results, the morphology of DPPT-TT films is considered to not drastically change when the annealing temperature is less than 200 °C.

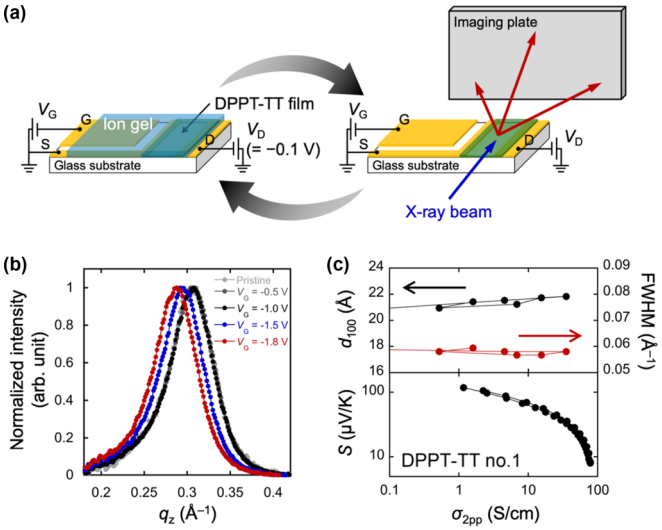

FIG. 6. GIXD measurements combined with electrolyte-gating transistors. (a) Optical photograph of the measurement setup and schematic illustration of the experimental procedure. (b) Normalized (100) peaks as a function of the wave number vector, q_z, at different gate voltages (V_G) in the DPPT-TT electrolyte-gated transistor. The spectrum of the pristine state is also indicated. (c) Two-point-probe electrical conductivity dependence of the full width at half maximum (FWHM) of the (100) peak. The S-σ_{2pp} relationship of DPPT-TT (sample no. 1) is also indicated.

APPENDIX B: GRAZING-INCIDENCE X-RAY DIFFRACTION (GIXD) MEASUREMENTS COMBINED WITH THE ELECTROLYTE-GATING TECHNIQUE

To evaluate the effect of carrier doping on the film morphology, we combined GIXD measurements with the electrolyte-gating transistor technique [14]. The GIXD measurements were performed using a Rigaku FR-E microfocus high intensity x-ray generator system with a CuKa x-ray source ($\lambda = 1.5418$ Å) in ambient air at the High Intensity X-ray Diffraction Laboratory at Nagoya University. For this experiment, we prepared electrolyte-gated transistors of large DPPT-TT films, in which the channel length and the channel width were 2 and 10 mm, respectively. Figure 6(a) shows an optical photograph of the measurement setup and a schematic illustration of the experimental procedure. First, we applied a gate voltage and simultaneously monitored the transistor properties. After observing the saturation of the drain current, we removed the ion gel film. Second, we performed GIXD measurements for 10 minutes and then replaced the ion gel film. We repeated these measurement steps to collect the gate-voltage dependence of the XRD profiles. It should be noted that we succeeded in tracing the relationship between the structural and electrical properties in the same DPPT-TT film using the electrolyte-gating transistor method.

Figure 6(b) presents the normalized (100) peaks as a function of the wave number vector, q_z, at various gate voltages. As shown in Fig. 6(b), the (100) peak continuously shifts to lower values as the negative gate voltage increases, indicating a change in the interlamellar distance due to the intercalation of anion molecules. The observed peak structure, however, seems to be constant upon carrier doping.

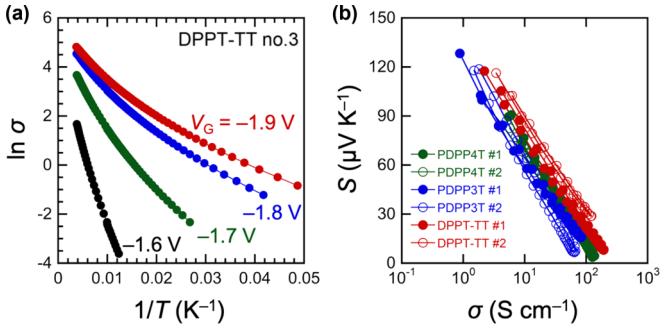

FIG. 7. Arrhenius plot and Jonker plot of the S-σ relationships in D-A copolymer electrolyte-gating transistors. (a) Arrhenius plots obtained from the DPPT-TT electrolyte-gated transistor (sample no. 3). (b) Jonker plot of the S-σ relationships in DPPT-TT, PDPP3T, and PDPP4T.

Figure 6(c) summarizes the electrical conductivity dependence of the full width at half maximum (FWHM) of the (100) peaks shown in Fig. 6(b). The S-σ_{2pp} relationship of DPPT-TT (sample no. 1) is also indicated. As shown in Fig. 6(c), the interlamellar distance expands from 20 to 22 Å, indicating that the calculated electrical conductivity in the present study is slightly overestimated. On the other hand, since the value of the FWHM of the (100) peaks is significantly small, it is suggested that the intercalation of anion molecules does not disturb the structure of the crystalline domain in the DPPT-TT film.

APPENDIX C: ARRHENIUS PLOT AND JONKER PLOT

Figure 7(a) shows the Arrhenius plot (i.e., ln σ vs $1/T$) obtained from the temperature dependences of the four-point-probe electrical conductivity in the DPPT-TT electrolyte-gated transistor (sample no. 3). If the carrier transport mechanism of DPPT-TT films is explained by thermally activated hopping transport, then one can see a linear relationship between ln σ and $1/T$. However, as shown in Fig. 7(a), such linear behavior is not observed for all measured gate voltages. Furthermore, Fig. 7(b) summarizes the S-σ relationships in D-A copolymer films (sample no. 1 and sample no. 2) on a semilogarithmic scale (the Jonker plot). In addition, Table II summarizes the slope values of the S-log σ trends. As shown in Fig. 7(b), even though linear behavior is observed in D-A copolymer films, the slope value is lower than the theoretical value in the Jonker plot (–198 μ V K^{-1}), as summarized in

TABLE II. Slope values between S and log σ in D-A copolymer films.

Sample	Slope value of S-log σ plot
DPPT-TT no. 1	–56
DPPT-TT no. 2	–57
PDPP3T no. 1	–54
PDPP3T no. 2	–69
PDPP4T no. 1	–62
PDPP4T no. 2	–53
Theoretical value	–198

TABLE III. Summary of the exponent n.

Dimension, d	$D(E) \propto$ const. ($\mu = 0$)	$D(E) \propto \lvert E–E_F \rvert$ ($\mu = 1$)	$D(E) \propto (E–E_F)^2$ ($\mu = 2$)
3	1/4	2/5	1/2
2	1/3	1/2	3/5
1	1/2	2/3	3/4

TABLE IV. Summary of the values of $x\{= 2/[n(1 + d)]\}$.

Dimension, d	$D(E) \propto$ const. ($\mu = 0$)	$D(E) \propto \lvert E–E_F \rvert$ ($\mu = 1$)	$D(E) \propto (E–E_F)^2$ ($\mu = 2$)
3	2	5/4	1
2	2	4/3	10/9
1	2	3/2	4/3

Table II [7,8]. Therefore, it is concluded that the thermally activated transport model is not suitable for the charge transport mechanism of D-A copolymer films.

APPENDIX D: THEORETICAL S-σ RELATIONSHIP FOR THE VARIABLE RANGE HOPPING TRANSPORT SYSTEM

In this section, we attempt to derive the theoretical S-σ relationship in the variable range hopping (VRH) transport system from conventional theory. First, within the theory of VRH transport, the temperature (T) dependence of the electrical conductivity (σ) is expressed as

$$\sigma(T) = \sigma_0 \exp\left[-\left(\frac{T_0}{T}\right)^n\right], \tag{D1}$$

where σ_0 is a temperature-independent factor and T_0 is interpreted as an effective energy separation between localized states [36,37]. In particular, considering the energy-dependent density of states [i.e., $D(E) \propto (E–E_F)^\mu$] due to the Coulomb gap, the exponent n in Eq. (D1) is generally described as [37,41]

$$n = \frac{1+\mu}{1+\mu+d}. \tag{D2}$$

Here, μ takes values of 0, 1, and 2, and d is the system dimensionality. According to Eq. (D2), Table III summarizes the value of n for various pairs of (d, μ).

Next, the Seebeck coefficient in the VRH system is theoretically described as [39]

$$S = \frac{k_B}{2e}\frac{E_h^2}{k_B T}\left.\frac{\partial \ln \sigma_E(E)}{\partial E}\right|_{E=E_F}, \tag{D3}$$

where k_B, e, E_h, and σ_E are the Boltzmann constant, the elementary charge, the energy transported by hopping carriers, and the spectrum conductivity, respectively. Based on the Mott doctrine, E_h is given by [39]

$$E_{h(\mathrm{Mott})} = \frac{1}{1+d} k_B (T_0 T^d)^{\frac{1}{1+d}}. \tag{D4}$$

By substituting Eqs. (D1) and (D4) into Eq. (D3), the theoretical S-σ relationship in the VRH transport system is predicted to be

$$S_{\mathrm{Mott}} = \frac{k_B^2 T}{2e}\frac{1}{(1+d)^2}\left(-\ln\frac{\sigma}{\sigma_0}\right)^{\frac{2}{n(1+d)}}\left.\frac{\partial \ln \sigma_E(E)}{\partial E}\right|_{E=E_F}. \tag{D5}$$

Under the condition of a constant $(\partial \ln \sigma_E(E_F)/\partial E)$, if $2/(n(1+d))$ is written as x, then one can see an x-power-law relationship between S and $|\ln \sigma/\sigma_0|$ from Eq. (D5). Table IV summarizes the values of x for various pairs of (d, μ).

In the case of the Efros-Shklobskii (ES) VRH model, the σ-T relationship and E_h are given by

$$\sigma(T) = \sigma_0 \exp\left[-\left(\frac{T_0}{T}\right)^{\frac{1}{2}}\right], \tag{D6}$$

$$E_{h(\mathrm{ES})} = \frac{1}{2} k_B (T_0 T)^{\frac{1}{2}}, \tag{D7}$$

regardless of the system dimensionality [37]. Consequently, by substituting Eqs. (D6) and (D7), Eq. (D3) becomes

$$S_{\mathrm{ES}} = \frac{k_B^2 T}{8e}\left(-\ln\frac{\sigma}{\sigma_0}\right)^2\left.\frac{\partial \ln \sigma_E(E)}{\partial E}\right|_{E=E_F}. \tag{D8}$$

[1] E. W. Zaia, M. P. Gordon, P. Yuan, and J. J. Urban, Progress and perspective: Soft thermoelectric materials for wearable and internet-of-things applications, Adv. Electron. Mater. **5**, 1800823 (2019).

[2] K. Kanahashi, J. Pu, and T. Takenobu, 2D materials for large-area flexible thermoelectric devices, Adv. Energy Mater. **10**, 1902842 (2019).

[3] J.-H. Bahk, H. Fang, K. Yazawa, and A. Shakouri, Flexible thermoelectric materials and device optimization for wearable energy harvesting, J. Mater. Chem. C **3**, 10362 (2015).

[4] C. Zheng, L. Xiang, W. Jin, H. Shen, W. Zhao, F. Zhang, C. Di, and D. Zhu, A flexible self-powered sensing element with integrated organic thermoelectric generator, Adv. Mater. Technol. **4**, 1900247 (2019).

[5] S. Hwang, W. J. Potscavage Jr., R. Nakamichi, and C. Adachi, Processing and doping of thick polymer active layers for flexible organic thermoelectric modules, Org. Electron. **31**, 31 (2016).

[6] O. Bubnova, Z. U. Khan, A. Malti, S. Braun, M. Fahlman, M. Berggren, and X. Crispin, Optimization of the thermoelectric figure of merit in the conducting polymer poly(3,4-ethylenedioxythiophene), Nat. Mater. **10**, 429 (2011).

[7] A. F. Ioffe, *Semiconductors Thermoelements and Thermoelectric Cooling* (Infoscarch Limited, London, 1957).

[8] C. Wood, Materials for thermoelectric energy conversion, Rep. Prog. Phys. **51**, 459 (1988).

[9] W. Shi, J. Ye, J. G. Checkelsky, C. Terakura, and Y. Iwasa, Transport properties of polymer semiconductor controlled by

ionic liquid as a gate dielectric and a pressure medium, Adv. Funct. Mater. **24**, 2005 (2014).

[10] S. Wang, M. Ha, M. Manno, C. D. Frisbie, and C. Leighton, Hopping transport and the Hall Effect near the insulator-metal transition in electrochemically gated poly(3-hexylthiophene) transistors, Nat. Commun. **3**, 1210 (2012).

[11] C. O. Yoon, Reghu M., D. Moses, and A. J. Heeger, Transport near the metal-insulator transition: Polypyrrole doped with PF_6, Phys. Rev. B **49**, 10851 (1994).

[12] S. D. Kang and G. J. Snyder, Charge-transport model for conducting polymers, Nat. Mater. **16**, 252 (2017).

[13] A. M. Graudell, J. E. Cochran, S. N. Patel, and M. L. Chabinyc, Impact of the doping method on conductivity and thermopower in semiconducting polythiophenes, Adv. Energy Mater. **5**, 1401072 (2015).

[14] H. Tanaka, K. Kanahashi, N. Takekoshi, H. Mada, H. Ito, Y. Shimoi, H. Ohta, and T. Takenobu, Thermoelectric properties of a semicrystalline polymer doped beyond the insulator-to-metal transition by electrolyte gating, Sci. Adv. **6**, eaay8065 (2020).

[15] H. Matsui, D. Kumaki, E. Takahashi, K. Takimiya, S. Tokito, and T. Hasegawa, Correlation between interdomain carrier hopping and apparent mobility in polycrystalline organic transistors as investigated by electron spin resonance, Phys. Rev. B **85**, 035308 (2012).

[16] S. Y. Son, Y. Kim, J. Lee, G.-Y. Lee, W.-T. Park, Y.-Y. Noh, C. E. Park, and T. Park. High-field-effect mobility of low-crystallinity conjugated polymers with localized aggregates, J. Am. Chem. Soc. **138**, 8096 (2016).

[17] H. Tanaka, A. Wakamatsu, M. Kondo, S. Kawamura, S.-I. Kuroda, Y. Shimoi, W.-T. Park, Y.-Y. Noh, and T. Takenobu, Microscopic observation of efficient charge transport processes across domain boundaries in donor-acceptor-type conjugated polymers, Commun. Phys. **2**, 96 (2019).

[18] D. Venkateshvaran, M. Nikolka, A. Sadhanala, V. Lemaur, M. Zelazny, M. Kepa, M. Hurhangee, A. J. Kronemeijer, V. Pecunia, I. Nasrallah *et al.*, Approaching disorder-free transport in high-mobility conjugated polymers, Nature (London) **515**, 384 (2014).

[19] X. Zhang, H. Bronstein, A. J. Kronemeijer, J. Smith, Y. Kim, R. J. Kline, L. J. Richterr, T. D. Anthopoulos, J. Sirringhaus, K. Song *et al.*, Molecular origin of high field-effect mobility in an indacenodithiophene-benzothiadiazole copolymer, Nat. Commun. **4**, 2238 (2013).

[20] C. B. Nielsen, M. Turbiez, and I. McCulloch, Recent advances in the development of semiconducting DPP-containing polymers for transistor applications, Adv. Mater. **25**, 1859 (2013).

[21] R. Noriega, J. Rivnay, K. Vandewal, F. P. V. Koch, N. Stingelin, P. Smith, M. F. Toney, and A. Salleo, A general relationship between disorder, aggregation and charge transport in conjugated polymers, Nat. Mater. **12**, 1038 (2013).

[22] S. Frantini, M. Nikolka, A. Salleo, G. Schweicher, and H. Sirringhaus, Charge transport in high-mobility conjugated polymers and molecular semiconductors, Nat. Mater. **19**, 491 (2020).

[23] Y. Li, S. P. Singh, and P. Sonar, A high mobility P-type DPP-thieno[3,2-b]thiophene copolymer for organic thin-film transistors, Adv. Mater. **22**, 4862 (2010).

[24] X. Zhang, L. J. Richter, D. M. DeLongchamp, R. J. Kline, M. R. Hammond, I. McCulloch, M. Heeney, R. S. Ashraf, J. N. Smith, T. D. Anthopoulos *et al.*, Molecular packing of high-mobility diketo pyrrolo-pyrrole polymer semiconductors with branched alkyl side chains, J. Am. Chem. Soc. **133**, 15073 (2011).

[25] Z. Chen, M. J. Lee, R. S. Ashraf, Y. Gu, S. Albert-Seifried, M. M. Nielsen, B. Schroeder, T. D. Anthopoulo, M. Heeney, I. McCulloch, and H. Sirringhaus, High-performance ambipolar diketopyrrolopyrrole-thieno[3,2-b]thiophene copolymer field-effect transistors with balanced hole and electron mobilities, Adv. Mater. **24**, 647 (2012).

[26] A. F. Paterson, S. Singh, K. J. Fallon, T. Hodsden, Y. Han, B. C. Schroeder, H. Bronstein, M. Heeney, I. McCulloch, and T. D. Anthopoulos, Recent progress in high-mobility organic transistors: A reality check, Adv. Mater. **30**, 1801079 (2018).

[27] M. Kim, S. U. Ryu, S. A. Park, K. Choi, T. Kim, D. Chung, and T. Park, Donor-acceptor-conjugated polymer for high-performance organic field-effect transistors: A progress report, Adv. Funct. Mater. **30**, 1904545 (2020).

[28] S. R. Chaudhari, J. M. Griffin, K. Broch, A. Lesage, V. Lemaur, D. Dudenko, Y. Oliver, H. Sirringhaus, L. Emsley, and C. P. Grey, Donor-acceptor stacking arrangements in bulk and thin-film high-mobility conjugated polymers characterized using molecular modelling and MAS and surface-enhanced solid-state NMR spectroscopy, Chem. Sci. **8**, 3126 (2017).

[29] H. Tanaka, S. Kawamura, P. Sonar, Y. Shimoi, T. T. Do, and T. Takenobu, Highly efficient microscopic charge transport within crystalline domains in a furan-flanked diketopyrrolopyrrole-based conjugated copolymer, Adv. Funct. Mater. **30**, 2000389 (2020).

[30] H. Sirringhaus, 25th anniversary article: Organic field-effect transistors: The path beyond amorphous silicon, Adv. Mater. **26**, 1319 (2014).

[31] A. Pickett, M. Torkkeli, T. Mukhopadhyay, B. Puttaraju, A. Laudari, A. E. Lauritzen, O. Bikondoa, J. K.-Hansen, M. Knaapila, S. Patil, and S. Guha, Correlating charge transport with structure in deconstructed diketopyrrolopyrrole oligomers: A case study of a monomer in field-effect transistors, ACS Appl. Mater. Interfaces **10**, 19844 (2018).

[32] F. Zhang, Y. Zang, D. Huang, C. Di, X. Gao, H. Sirringhaus, and D. Zhu, Modulated thermoelectric properties of organic semiconductors using field-effect transistors, Adv. Funct. Mater. **25**, 3004 (2015).

[33] A. Salleo, R. J. Kline, D. M. DeLongchamp, and M. L. Chabinyc, Microstructural characterization and charge transport in thin films of conjugated polymers, Adv. Mater. **22**, 3812 (2010).

[34] I. McCulloch, M. Heeney, C. Bailey, K. Genevicius, I. MacDonald, M. Shkunov, D. Sparrowe, S. Tierrney, R. Wagner, W. Zhang *et al.*, Liquid-crystalline semiconducting polymers with high charge-carrier mobility, Nat. Mater. **5**, 328 (2006).

[35] K. Kanahashi, M. Ishihara, M. Hasegawa, H. Ohta, and T. Takenobu, Giant power factors in p- and n-type large-area graphene films on a flexible plastic substrate, npj 2D Mater. Appl. **3**, 44 (2019).

[36] N. F. Mott and E. Davis, *Electronic Processes of Non-Crystalline Material* (Clarendon Press, Oxford, 1979).

[37] B. I. Shklovskii and A. L. Efros, *Electronic Properties of Doped Semiconductors* (Springer-Verlag, Heidelberg, 1984).

[38] A. G. Zabrodskii and K. N. Zinov'eva , Low-temperature conductivity and metal-insulator transition in compensate n-Ge,

Zh. Eksp. Teor. Fiz. **86**, 727 (1984) [Sov. Phys. JETP **59**, 426 (1984)].

[39] M. J. Burns and P. M. Chaikin, Interaction effects and thermoelectric power in low-temperature hopping, J. Phys. C: Solid State Phys. **18**, L743 (1985).

[40] We used different samples for collecting the data of the room-temperature S-σ relationship (samples no. 1 and no. 2) and the temperature dependence of σ (sample no. 3). First, from the $\sigma(T)$ data of sample no. 3, we obtained the room-temperature σ values ($\sigma_{300\mathrm{K}}$) and σ_0 at different gate voltages. Then, from the S-σ relationships of sample no. 1 and sample no. 2, we estimated the room-temperature Seebeck coefficients of sample no. 3 at different gate voltages. These results are summarized in Table I.

[41] T. Chen and B. Skinner, Enhancement of hopping conductivity by spontaneous fractal ordering of low-energy sites, Phys. Rev. B **94**, 085146 (2016).